APPROVAL SHEET

Title of Thesis: Development and Analysis of a Quantitative Mathematical Model of Bistability in the Cross Repression System Between APT and SLBO Within the JAK/STAT Signaling Pathway

Name of Candidate: Alyssa Berez
Master of Science in Applied Mathematics, 2019

Thesis and Abstract Approved: _____
Dr. Bradford Peercy
Associate Professor
Department of Mathematics and Statistics

Date Approved: _____

ABSTRACT

Title of dissertation: DEVELOPMENT AND ANALYSIS OF A QUANTITATIVE MATHEMATICAL MODEL OF BISTABILITY IN THE CROSS REPRESSION SYSTEM BETWEEN APT AND SLBO WITHIN THE JAK/STAT SIGNALING PATHWAY

Alyssa Berez, Master of Science, 2019

Dissertation directed by: Professor Bradford Peercy
Department of Mathematics and Statistics

Cell migration is a key component in development and pathology. Inhibition of STAT activity by APT and cross-repression of APT and SLBO determines whether a border cell in the *Drosophila* oocyte becomes motile or remains stationary. Through mathematical modeling and analysis, we examine how the interaction of STAT, APT, and SLBO creates bistability in the JAK/STAT signaling pathway. In this paper, we update and analyze the mechanistic Ge and Stonko model to best represent the processes of the JAK/STAT pathway. We utilize parameter, bifurcation, and phase plane analysis, and make reductions to the system to produce a minimal quantitative model. We achieve this by combining two subsystems of differential equations. The subsystem with dynamic APT and SLBO has the necessary elements for bistability. The subsystem with dynamic STAT monomer and

activated STAT dimers incorporates how APT inhibits STAT. We found these two subsystems capture well the interaction of STAT, APT and SLBO in a four-variable model.

DEVELOPMENT AND ANALYSIS OF A QUANTITATIVE MATHEMATICAL MODEL OF BISTABILITY IN THE CROSS REPRESSION SYSTEM BETWEEN APT AND SLBO WITHIN THE JAK/STAT SIGNALING PATHWAY

by

Alyssa Berez

Thesis submitted to the Faculty of the Graduate School of the
University of Maryland, Baltimore County in partial fulfillment
of the requirements for the degree of
Master of Science
2019

Dedication

To Mom, Dad, and Jaime

Acknowledgments

I would like to thank my thesis director, Dr. Peercy, for all of his help and guidance. I would also like to thank my committee members, Dr. Starz-Gaiano, and Dr. Hoffman.

I would like to acknowledge the previous work done within the NSF-funded UBM program at UMBC that forms the basis of this thesis.

Table of Contents

List of Tables

List of Figures

1

Introduction

1.1 JAK/STAT Pathway

The process of cellular migration plays a critical role in both normal and pathological development. A better understanding of the processes cells undergo as they transition from a stationary state to a migratory state is thus of broad interest. To study cell migration, some scientists turn to an experimental model system. In *Drosophila melanogaster*, a set of cells called border cells develop during oogenesis and later become migratory, traveling through the egg chamber to the oocyte. Experimentalists have refined how this process occurs and what causes some border cells to become motile while others remain stationary, including the primary biochemical and molecular pathways. We are interested in advancing a mathematical model of these pathways, which could have implications on acquisition of cell motility in animals in general.

The Janus Kinase/Signal Transducer and Activator of Transcription (JAK/STAT) signaling pathway has been shown by previous studies to be crucial in the motility of border cells [14]. Anterior polar cells in the *Drosophila* egg chamber (see Figure 1.1) secrete the cytokine Unpaired (UPD), which acts as the ligand for the transmembrane Domeless receptor in neighboring follicle cells. The binding of Unpaired to Domeless activates JAK, leading to the phosphorylation of the the activated

JAK/receptor complex. The activated JAK-receptor complex then recruits and phosphorylates STAT. The phosphorylated STAT dimerizes, moves to the nucleus, and acts as a transcription factor for specific target genes. The individual border cells are signaled by UPD which forms a gradient across the adjacent border cells. The cells receiving sufficiently high levels of UPD, not necessarily just those in closer proximity to the polar cells depending on the extracellular geometry [8], turn on a higher level of STAT activity. This in turn promotes their transformation into mobile border cells.

We focus on the proteins of two genes targeted by STAT: Apontic (APT) and Slow Border Cells (SLBO). APT protein is a transcription factor that represses the function of JAK/STAT and SLBO, and thus inhibits migration [12]. Earlier studies show that APT acts as a feedback inhibitor on the JAK/STAT pathway, and that this process is mediated by APT's activation of a microRNA that reduce STAT protein through various processes [16]. APT also activates expression of Socs36E, which blocks STAT signalling via a degradation pathway [9]. SLBO promotes migratory behavior and an insufficient amount of SLBO prevents motility [10]. APT and SLBO also exhibit cross-repressional behavior [12]. APT directly represses SLBO transcription while SLBO only decreases the level of expression of APT protein. The dominating protein in a given cell determines the cell fate: stationary or motile.

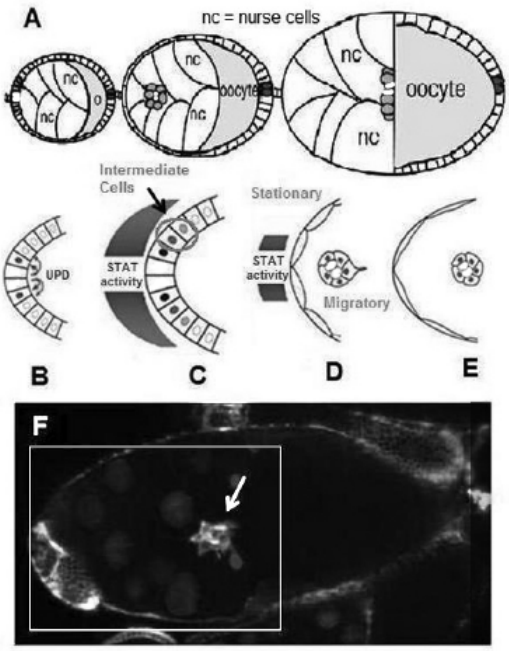

Figure 1.1: Egg development and the migration of border cells. (A) A cartoon of the development of a *Drosophila* egg chamber and the movement of the border cells between the nurse cells (nc). (B) The signaling molecule Unpaired is secreted from the polar cells and (C) induces a gradient of STAT activity across the anterior epithelium. Often the follicle cells very close to the polar cells assume the identity of border cells, (D) become motile, and (E) migrate towards the oocyte. (F) is a Fluorescent Protein-STAT reporter [1] staining of a wild type egg chamber, which demonstrates that STAT transcriptional activity is highest in the migrating border cell cluster (arrow). Adapted from [2].

1.2 Ge and Stonko Model

We base our model on the mechanistic model built by Ge and Stonko (2012). Focusing on the cross-repression system of APT and SLBO, they built a mathematical model using elementary interactions to identify which components of the system are sufficient for bistability. A rapid transition into motility is observed. We interpret this as a bistable switch. Depending on the strength of the Unpaired signal and

thus the level of STAT activity, each border cell can become motile (SLBO dominated) or remain stationary (APT dominated). Cells with an intermediate level of STAT may fall above or below the threshold of STAT necessary for mobility.

Ge and Stonko focused on the cross-repression system of APT and SLBO (shown in Figure 1.2) and created a system with sufficient elements, specifically cooperativity in SLBO repressing APT mRNA, to cause bistability.

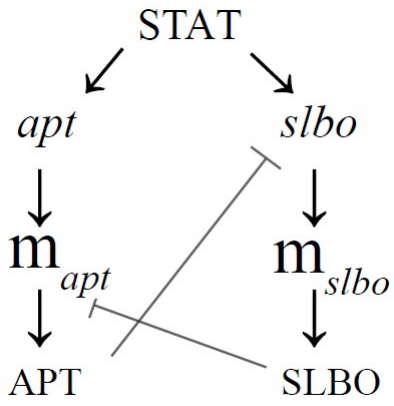

Figure 1.2: Cross-repression system of APT and SLBO. STAT activates *apt* and *slbo* transcription leading to the production of *apt* and *slbo* mRNA and translation into APT and SLBO proteins. SLBO represses *apt* translation while APT suppresses *slbo* transcription and function.

The level of STAT is treated as a parameter. The variables are listed in Table 1.1.

Variable	Description
A	Amount of APT protein
B	Amount of SLBO protein
m_α	Amount of APT mRNA
m_β	Amount of SLBO mRNA
α	Proportion of inactive apt genes
β	Proportion of inactive slbo genes
β^R	Proportion of repressed slbo genes

Table 1.1: Seven-variable model variables

We first consider the seven equations down stream of STAT activation. The original parameter values in this model were assigned to obtain the bistability expected from the data and qualitative nature of the model.

The seven variable model is

$$\frac{dA}{dt} = k_A m_\alpha - \delta_A A \tag{1.1}$$

$$\frac{dB}{dt} = k_B m_\beta - \delta_B B \tag{1.2}$$

$$\frac{dm_\alpha}{dt} = k_{m_\alpha}(1-\alpha) - \delta_{m_\alpha} m_\alpha + m_\alpha^o - \delta_{B\alpha} B^2 m_\alpha \tag{1.3}$$

$$\frac{dm_\beta}{dt} = k_{m_\beta}(1-\beta-\beta^R) - \delta_{m_\beta} m_\beta + m_\beta^o - \delta_{A\beta} A m_\beta \tag{1.4}$$

$$\frac{d\alpha}{dt} = -k_\alpha^f S_2^* \alpha + k_\alpha^b (1-\alpha) \tag{1.5}$$

$$\frac{d\beta}{dt} = -k_\beta^f S_2^* \beta + k_\beta^b (1-\beta-\beta^R) \tag{1.6}$$

$$\frac{d\beta^R}{dt} = k_{\beta^R}^f A\beta - k_{\beta^R}^b \beta^R \tag{1.7}$$

In this thesis we will analyze and adapt the Ge and Stonko model so that it quantifies the processes of the JAK/STAT pathway. We establish parameters and test bifurcation results, make reductions to the model, identify manifolds, reintroduce STAT dynamics, and test experimental results. We apply this model in the interesting case of controlling microRNA degradation of STAT via APT and show that delays in STAT activation, even to the point of activation failure within a biophysical time span, are possible due to the proximity of the critical UPD level to a limit point bifurcation.

2

Parameter and Bifurcation Analysis

2.1 Establishing Parameters

In order to establish a more biophysically realistic model for this study, we researched existing literature to find data to establish parameter values. For some parameters we were able to find data specific to the JAK/STAT pathway or *Drosophila*. For other parameters related pathways were used to obtain data relevant to this model.

We were able to identify published values for general translation and transcription rates and applied the established rates to the lengths of APT and SLBO genes and proteins [5, 7]. Protein and mRNA degradation rates have a wide range of average values so APT and SLBO are assumed to conform to this range [3, 6]. The binding and dissociation rates of STAT have been identified in general but not specifically to *apt* and *slbo* genes [4, 11, 15].

The details of kinetics of mRNA degradation due to microRNA (miRNA) have not been studied in detail and as such the corresponding parameters are difficult to assign. Ge and Stonko addressed this by condensing the various processes by which miRNA can affect mRNA into one degradation rate. We identified a parameter value for this combined effect through information from the model established in Yoon et al. (2011) and the fact that the model is fairly insensitive to this parameter.

The rate that SLBO transitions in and out of its repressed state was also hard to identify due to lack of data, so we utilized the rate given in Ge and Stonko which was adapted from Harris et al. (2011). Lastly, for the rates of STAT independent mRNA production we again used the original parameter values from Starz-Gaiano (2009). For *slbo*, this rate is most likely negligible. However, *apt* can be activated by means other than STAT. The protein Eyes Absent (EYA) can also activate transcription of *apt* [2].

Throughout the research on parameter values, the goal was to develop a range of realistic parameters to test. There are two reasons why a range of values is desirable. First, from the biological point of view, many biological processes do not occur at consistent rate. Additionally, heterogeneity will likely lead to some parameter variety. A range of average values is thus both more appropriate and more consistent with experimental data. Second, some degree of uncertainty in the parameters creates the opportunity for further mathematical analysis. We were able to test the robustness of the dynamics over the ranges of parameters to see if the model behavior matches experimentally observed outcomes.

We created subsets of parameters to test them. Parameters were grouped by the equation in which they appeared, then a bifurcation diagram was created in XPP/AUT to see if bistability was maintained from the original parameter set. The bifurcation parameter, as in the original study, was the level of activated STAT. As most parameters have a range of feasible values, some adjustment was necessary to preserve the system's bistability. After each group of parameters was set to create bistability, two-parameter bifurcations were performed for all parameters against

STAT level. This identified the range of values for each parameter that upheld bistability. The range of researched values identifies a robust region of bistability. This adds validity to the decision to use some parameter values that were established from a range of possible values.

Once each group of parameter values was confirmed to sustain bistability, the next set of parameters was tested. For example, the parameters in the protein equations were tested first and then the parameters in the mRNA equations were added. This sometimes necessitated changing previously set parameters, but for the most part earlier values could remain unchanged. The two-parameter bifurcations were repeated so as to refine the bistable ranges each time a new parameter value was established. Most of the time these ranges only slightly changed with each new parameter.

The parameter values established through research and testing for bistability are shown in Table 2.1.

Parameter	Symbol	Value	Units	Citation
Rate of APT translation	k_A	0.298	min^{-1}	[5, 7]
Rate of transcription of *apt*	k_{m_α}	0.54	nM*min^{-1}	[5, 7]
Rate of STAT independent production of *apt* mRNA	m_α^o	0.52	nM*min^{-1}	[13]
Rate of degradation of APT	δ_A	0.04	min^{-1}	[3, 6]
Rate of degradation of *apt* mRNA	δ_{m_α}	0.086	min^{-1}	[3, 6]
Degradation rate of *apt* mRNA due to miRNA	$\delta_{A\beta}$	0.1	$\text{nM}^{-1}\text{*min}^{-1}$	[16]
Binding rate of STAT to *apt*	k_α^f	100	min^{-1}	[4, 11, 15]
Dissociation rate of STAT to *apt*	k_α^b	0.66	nM*min^{-1}	[4, 11, 15]
Rate of SLBO translation	k_B	0.312	min^{-1}	[5, 7]
Rate of transcription of *slbo*	k_{m_β}	0.538	nM*min^{-1}	[5, 7]
Rate of STAT independent production of *slbo* mRNA	m_β^o	0.03	nM*min^{-1}	[13]
Rate of degradation of SLBO	δ_B	0.04	min^{-1}	[3, 6]
Rate of degradation of *slbo* mRNA	δ_{m_β}	0.086	min^{-1}	[3, 6]
Degradation rate of *slbo* mRNA due to miRNA	$\delta_{B\alpha}$	0.5	$\text{nM}^{-2}\text{*min}^{-1}$	[16]
Binding rate of STAT to *slbo*	k_β^f	100	min^{-1}	[4, 11, 15]
Dissociation rate of STAT to *slbo*	k_β^b	0.66	nM*min^{-1}	[4, 11, 15]
Rate *slbo* transitions into repressed state	$k_{\beta^R}^f$	100	min^{-1}	[6]
Rate *slbo* transitions out of repressed state	$k_{\beta^R}^b$	0.522	nM*min^{-1}	[6]

Table 2.1: Ge and Stonko seven-variable system parameter values.

The bistable range of each parameter is reported in Table 2.2.

Parameter	Bistable Start	Bistable End
k_A	0.04	0.615
k_{m_α}	0	1.67
m_α^o	0	1.65
δ_A	0.019	0.334
δ_{m_α}	0.024	24.5
$\delta_{A\beta}$	0.4	0.98
k_α^f	0	1098
k_α^b	0	998
k_B	0.144	1.56
k_{m_β}	0.232	985
m_β^o	0	0.243
δ_B	0.0011	0.08
δ_{m_β}	0	2.77
$\delta_{B\alpha}$	0.031	30.19
k_β^f	4.7	1094
k_β^b	0	14.02
$k_{\beta^R}^f$	0	1003
$k_{\beta^R}^b$	0	959

Table 2.2: Bistable Range of each parameter. Any value in this range will maintain bistability in the model with other parameters held at their baseline values from Table 2.1.

2.2 Bifurcation Analysis

A bifurcation diagram of APT against activated STAT (S_2^*) revealed a non-trivial state when $S_2^* = 0$ with a high level of APT, as seen in Figure 2.1. This can be interpreted as the system being predisposed to the stationary cell fate until STAT is high enough.

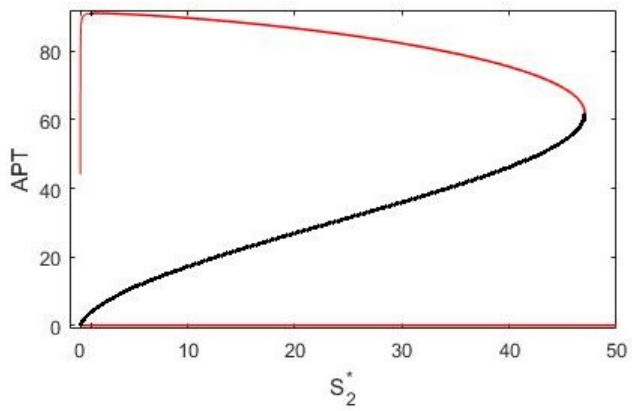

Figure 2.1: Bifurcation in seven-variable system of APT against STAT (S_2^*). Red indicates a stable steady state, black indicates an unstable steady state. Limit point bifurcations create 'knees' where the model jumps from one steady state to the other. At $S_2^* = 0$ APT dominates.

3

Reduced Models

3.1 Four-Variable Model

In the process of researching biophysically realistic parameters we discovered that the binding rate of STAT to target genes appears to be several orders of magnitude faster than any other process in the system [4, 11]. For example, k_{α}^{f}, k_{β}^{f}, and $k_{\beta^R}^{f}$ are at least three orders of magnitude faster than the other kinetics. Additionally, α, β, and β^R reach equilibrium significantly faster than the other variables. We used time-scale analysis to reduce the system. We made a quasi-steady state approximation for α, β, and β^R and set those derivatives equal to zero. This allowed us to solve equations (1.5). (1.6), and (1.7) for $\alpha^* = 1 - \alpha$ and $\beta^* = 1 - \beta - \beta^R$ in terms of APT protein and STAT dimer:

$$\alpha^* = \frac{\frac{S_2^*}{K_\alpha}}{\frac{S_2^*}{K_\alpha} + 1} \tag{3.1}$$

$$\beta = \frac{1}{\frac{S_2^*}{K_\beta} + 1 + \frac{A}{K_{\beta R}}} \tag{3.2}$$

$$\beta^R = \frac{k_{\beta^R}^f}{k_{\beta^R}^b} A\beta = \frac{\frac{A}{K_{\beta R}}}{\frac{S_2^*}{K_\beta} + 1 + \frac{A}{K_{\beta R}}} \tag{3.3}$$

$$\beta^* = 1 - \beta - \beta^R = \frac{\frac{S_2^*}{K_\beta}}{\frac{S_2^*}{K_\beta} + 1 + \frac{A}{K_{\beta R}}} \tag{3.4}$$

$$\text{with } K_\alpha = \frac{k_\alpha^b}{k_\alpha^f}, \quad K_\beta = \frac{k_\beta^b}{k_\beta^f}, \quad K_{\beta^R} = \frac{k_{\beta^R}^b}{k_{\beta^R}^f}$$

This creates a reduced system of four equations:

$$\frac{dA}{dt} = k_A m_\alpha - \delta_A A \tag{3.5}$$

$$\frac{dB}{dt} = k_B m_\beta - \delta_B B \tag{3.6}$$

$$\frac{dm_\alpha}{dt} = k_{m_\alpha}(\alpha^*) - \delta_{m_\alpha} m_\alpha + m_\alpha^o - \delta_{B\alpha} B^2 m_\alpha \tag{3.7}$$

$$\frac{dm_\beta}{dt} = k_{m_\beta}(\beta^*) - \delta_{m_\beta} m_\beta + m_\beta^o - \delta_{A\beta} A m_\beta \tag{3.8}$$

In order to compare the seven- and four-variable systems ((1.1)-(1.7) vs (3.5)-(3.8)) two cases were considered. First, the case where all gene binding and dissociation rates are several orders of magnitude faster than the other kinetics. In this case the seven- and four-variable systems exhibit similar dynamics, reaching nearly identical equilibria, as seen in Figures 3.1 and 3.2.

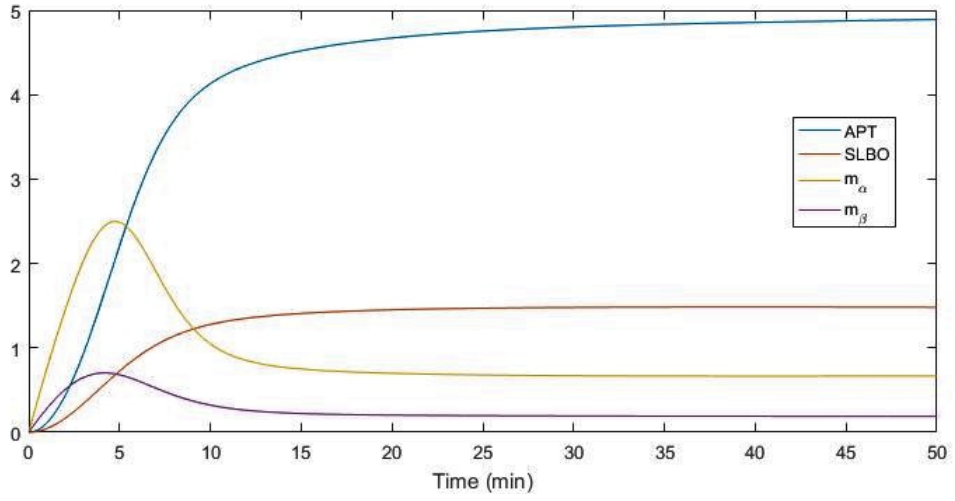

Figure 3.1: Time courses in seven-variable system with $S_2^* = 1$ and $k_\alpha^b = k_\beta^b = k_{\beta^R}^b = 100$.

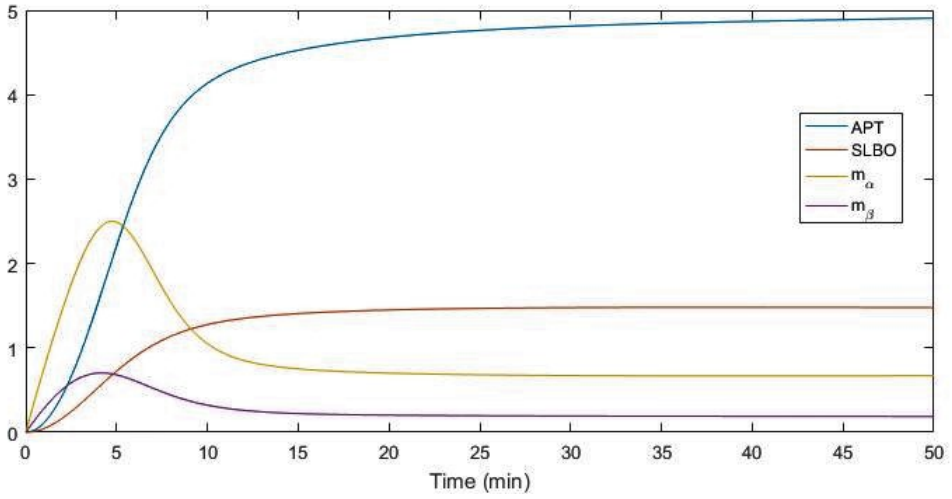

Figure 3.2: Time courses in four-variable system with $S_2^* = 1$ and $k_\alpha^b = k_\beta^b = k_{\beta^R}^b = 100$.

The other case assumes that only the forward genetic binding rates are significantly faster than the other kinetics. Here, for certain values of STAT, the two systems arrive at different steady states as shown in Figures 3.3 and 3.4.

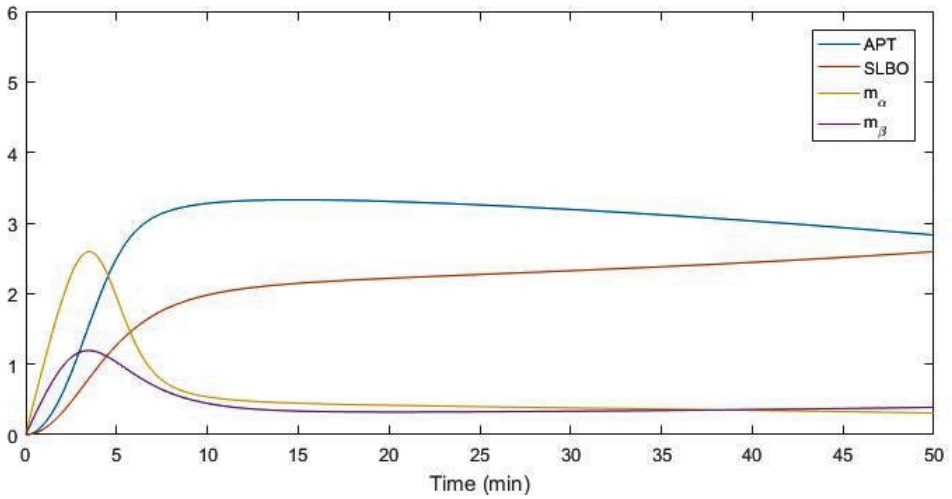

Figure 3.3: Time courses in seven-variable system with $S_2^* = 1$ and parameters from Table 2.1.

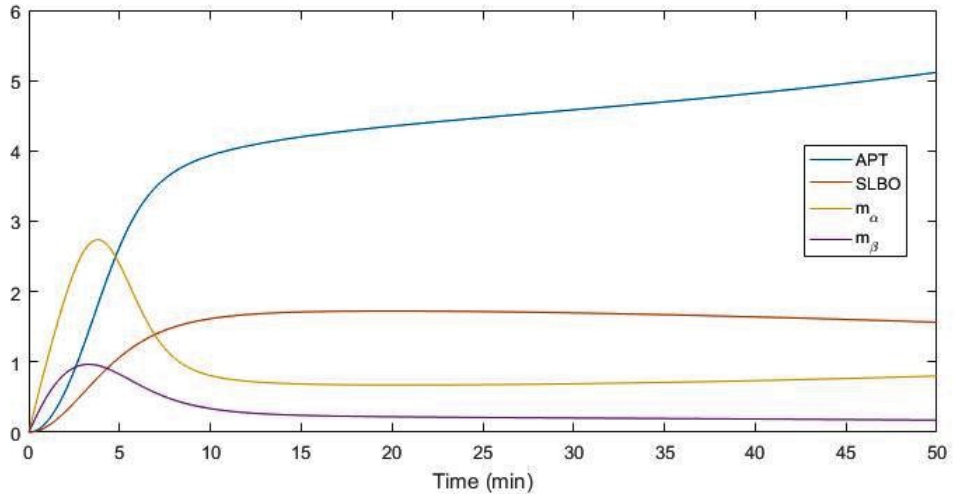

Figure 3.4: Time courses in four-variable system with $S_2^* = 1$ and parameters from Table 2.1.

Figures 3.3 and 3.4 use the baseline parameters from Table 2.1. For these parameters the manifold separating the basins of attraction of APT and SLBO changes in the reduction from the seven-variable model to the four-variable model.

3.2 Two-Variable Models

In order to better identify the manifold between the steady states, we attempted to reduce the four-variable system further to a system of two variables. Our parameter values indicate that the mRNA processes occur at least twice as fast as the protein processes. This makes a quasi-steady state approximation for m_α and m_β more plausible. For comparison, we also tested the results of a quasi-steady state approximation for A and B.

The dynamic protein model is

$$m_\alpha = \frac{k_{m_\alpha}(\alpha^*) + m_\alpha^o}{\delta_{m_\alpha} + \delta_{B\alpha}B^2} \tag{3.9}$$

$$m_\beta = \frac{k_{m_\beta}(\beta^*) + m_\beta^o}{\delta_{m_\beta} + \delta_{A\beta}A} \tag{3.10}$$

$$\frac{dA}{dt} = k_A\frac{k_{m_\alpha}(\alpha^*) + m_\alpha^o}{\delta_{m_\alpha} + \delta_{B\alpha}B^2} - \delta_A A \tag{3.11}$$

$$\frac{dB}{dt} = k_B\frac{k_{m_\beta}(\beta^*) + m_\beta^o}{\delta_{m_\beta} + \delta_{A\beta}A} - \delta_B B \tag{3.12}$$

The dynamic mRNA model is

$$A = \frac{k_\alpha m_\alpha}{\delta_A} \tag{3.13}$$

$$B = \frac{k_\beta m_\beta}{\delta_B} \tag{3.14}$$

$$\frac{dm_\alpha}{dt} = k_{m_\alpha}(\alpha^*) - \delta_{m_\alpha}m_\alpha + m_\alpha^o - \delta_{B\alpha}\left(\frac{k_\beta m_\beta}{\delta_B}\right)^2 m_\alpha \tag{3.15}$$

$$\frac{dm_\beta}{dt} = k_{m_\beta}(\beta^*) - \delta_{m_\beta}m_\beta + m_\beta^o - \delta_{A\beta}\frac{k_\alpha m_\alpha}{\delta_A}m_\beta \tag{3.16}$$

Both two-variable systems reach almost exactly the same equilibria and have identical bifurcation diagrams as the seven- and four-variable systems (as seen in Figure 2.1). However, the early behavior of the dynamic mRNA model is significantly different from that of the four-variable model. In the seven- and four-variable systems when a trajectory is close to a manifold there is a delay before it converges to equilibrium. By shifting the level of STAT to find trajectories close to the new manifolds, the time courses in the dynamic protein model show the delay seen in the

time courses of the four-variable system. Since the delay shown in Figure 3.6 can be obtained at $S_2^* = 1.895$, the exact delay seen in Figure 3.5 can also be obtained in the interval [1,1.895]. The delay seen in Figure 3.7 can not be attained in the dynamic mRNA model just by changing the value of STAT as shown in Figure 3.8.

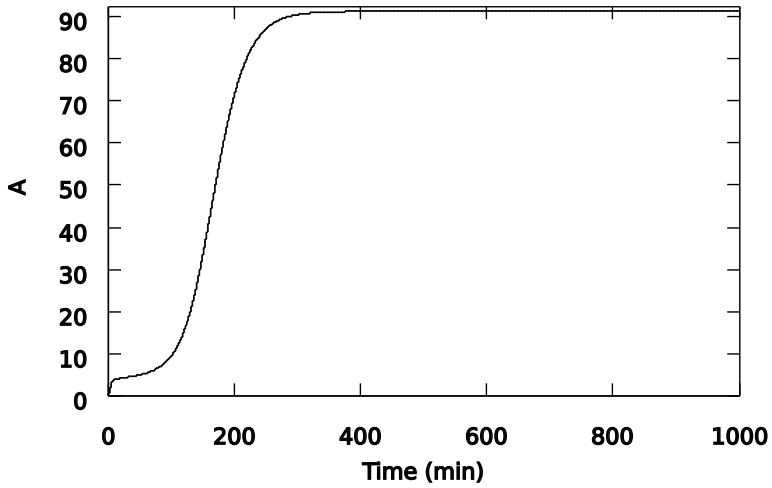

Figure 3.5: Time course of APT in four-variable system with $S_2^* = 1$, showing a delay.

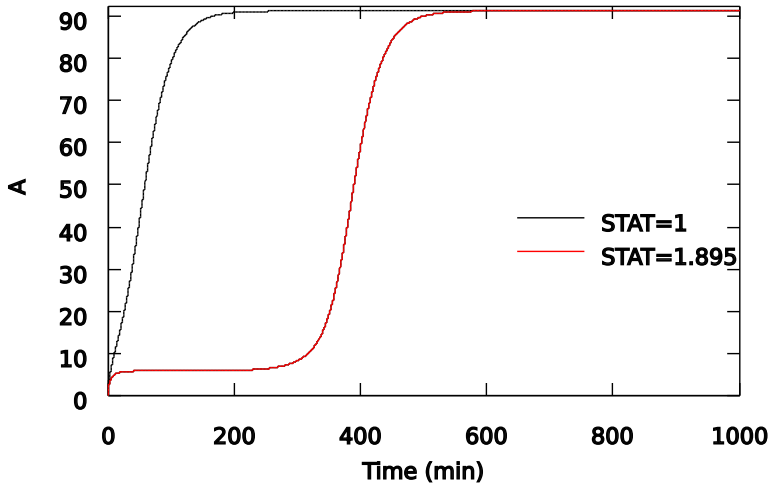

Figure 3.6: Time courses of APT in dynamic protein model. A shift to $S_2^* = 1.895$ creates a delay.

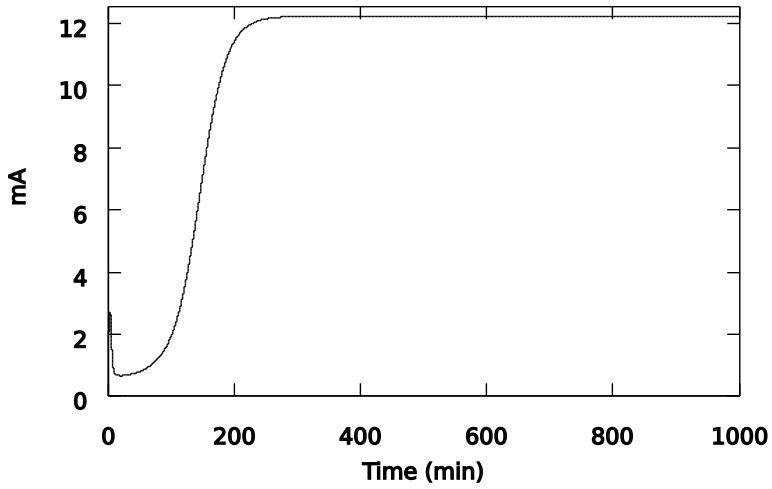

Figure 3.7: Time course of m_α in four-variable system with $S_2^* = 1$, showing a delay.

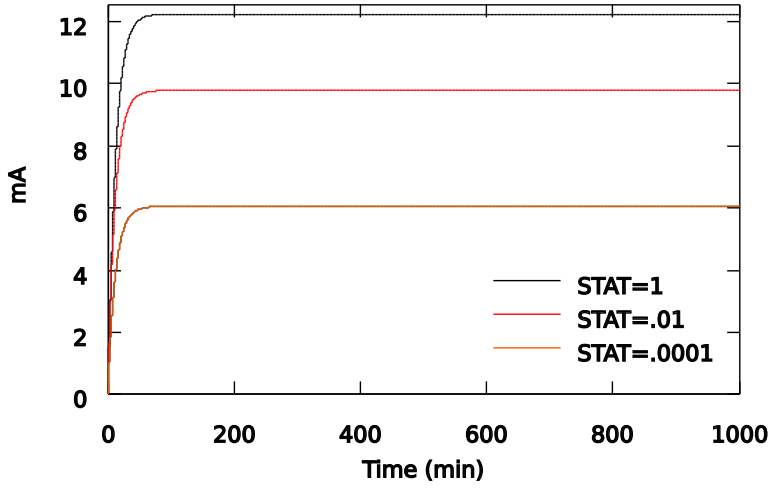

Figure 3.8: Time courses of m_α in dynamic mRNA model. No delay is created by shifting S_2^*.

3.3 Manifolds Separating APT and SLBO Basins of Attraction

While testing the four-variable model we discovered that for all initial conditions at 0, the same level of STAT converged to different steady states in the seven-variable model than in the four-variable model. This led us to investigate the manifold that separates the steady states in both systems. For a level of STAT in the bistable region, cells can either become motile or remain stationary depending on the initial conditions of the system. An example of this is given in Figure 3.9:

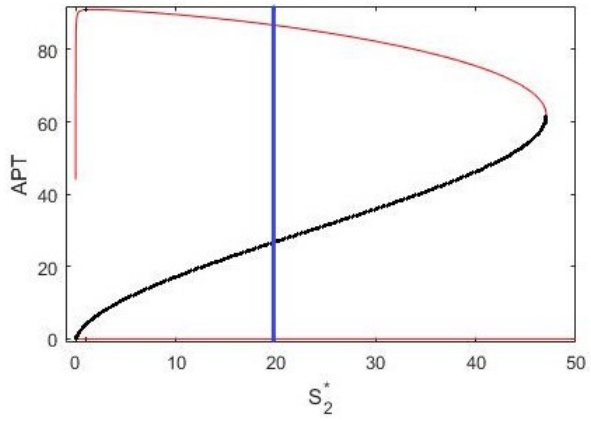

Figure 3.9: Bifurcation diagram of seven-variable system for APT against STAT (S_2^*), from Figure 2.1. The vertical line indicates S_2^*=20. At this level of STAT, either steady state can be reached depending on the initial conditions of the system.

We visually identified the manifolds by labeling initial conditions according to which steady state they converge. This allows us to see the basins of attraction for each steady state. These two stable steady states, one where SLBO dominates and the cell becomes motile and one where APT dominates and the cell remains stationary, are listed in Table 3.1 with values for each variable.

Variable	Steady State 1 (SS1): SLBO (Red)	Steady State 2 (SS2): APT (Blue)	Units
A	0.0062	91.062	nM
B	50.46	0.029	nM
m_α	0.000083	12.223	nM
m_β	6.469	0.0038	nM
α	0.00655	0.00655	Proportion of inactive genes
β	0.00651	0.0000568	Proportion of inactive genes
β^R	0.0077	0.991	Proportion of repressed genes

Table 3.1: Stable steady state values with $S_2^* = 1$ in the seven-variable model, (1.1)-(1.7).

In higher dimensional systems, identifying manifolds becomes difficult so we focus on two dimensional projections of the system. Trajectories plotted with the 3D bifurcation of APT and SLBO against STAT in the seven-variable system give us an idea of the manifold between the steady states (Figure 3.10).

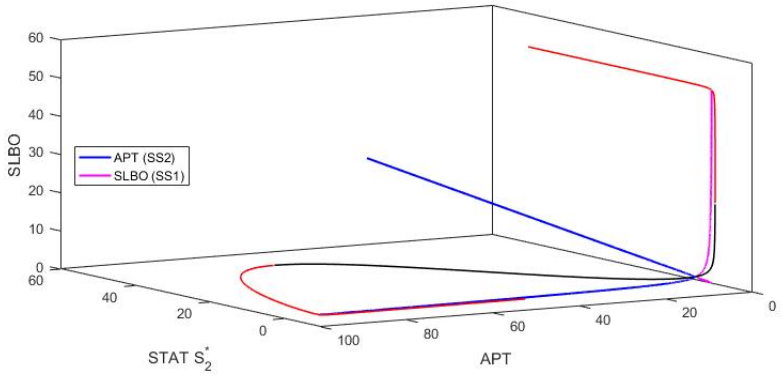

Figure 3.10: 3D bifurcation of APT and SLBO against STAT. Trajectory approaching SS1 has $S_2^* = 0.8$ and trajectory approaching has $S_2^* = 47$ with initial conditions A=80 and B=40.

We identified the projections of manifolds between the two stable equilibria in the m_α vs α and m_β vs β planes. We compared the seven- and four-variable systems for these planes with all other initial conditions fixed at 0. Figures 3.11 through 3.15 have $S_2^* = 1$, one of the values in a small range observed to converge to different steady states. Blue dots indicate the APT basin of attraction and red dots indicate the SLBO basin of attraction. The boundary between the basins of attraction approximates the manifold. Figures 3.11 and 3.12 show the m_α vs α plane and Figures 3.13 and 3.14 show the m_β vs β plane.

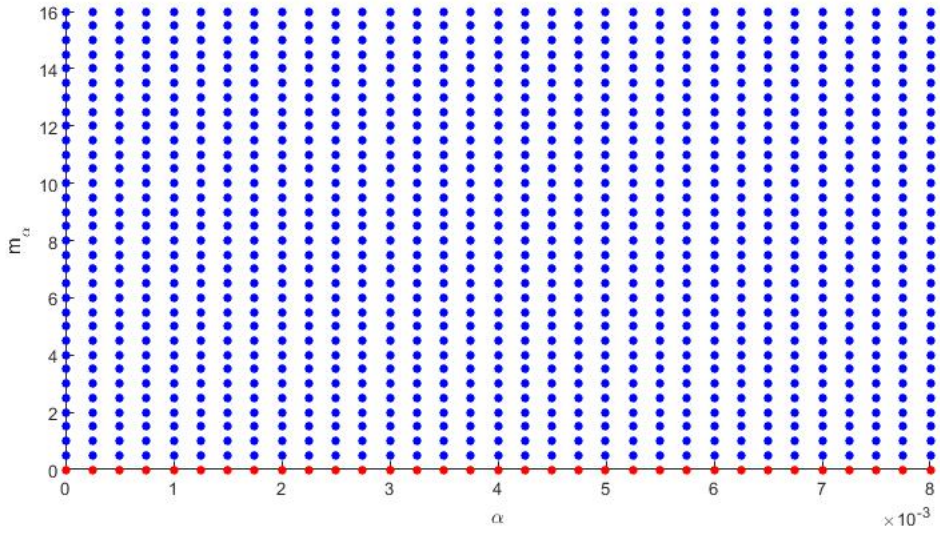

Figure 3.11: m_α vs α in the seven-variable system showing manifold.

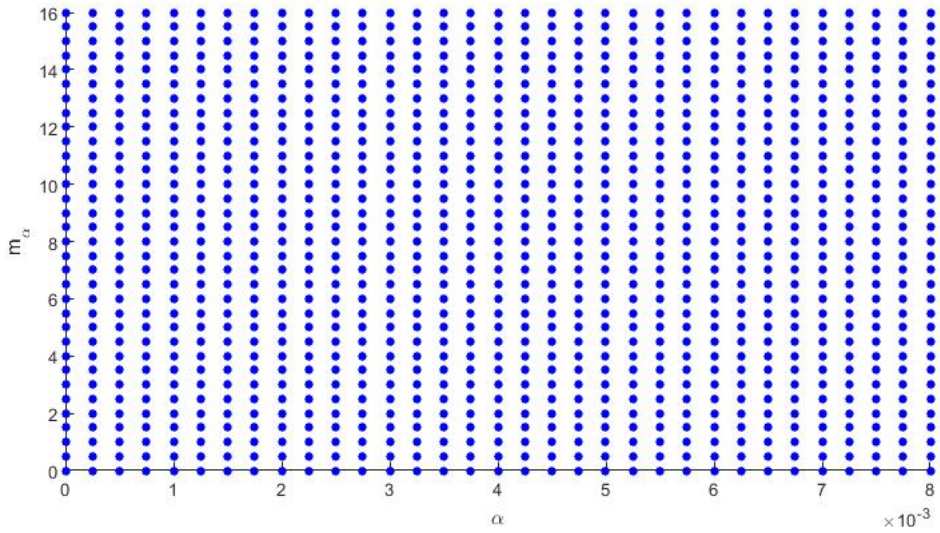

Figure 3.12: m_α vs α in the four-variable system showing no manifold.

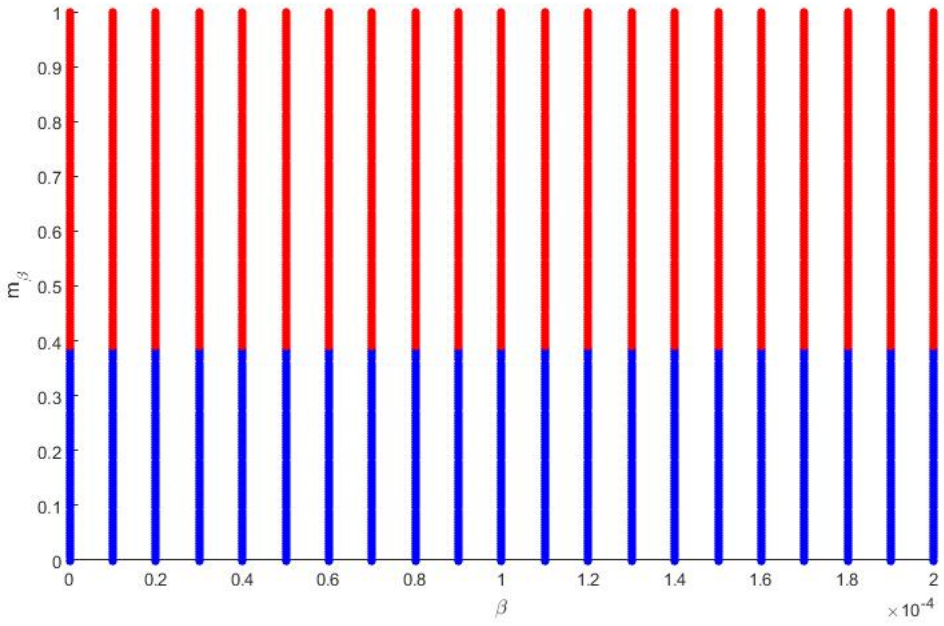

Figure 3.13: m_β vs β in the seven-variable system with initial condition of $m_\alpha = 1$ showing manifold.

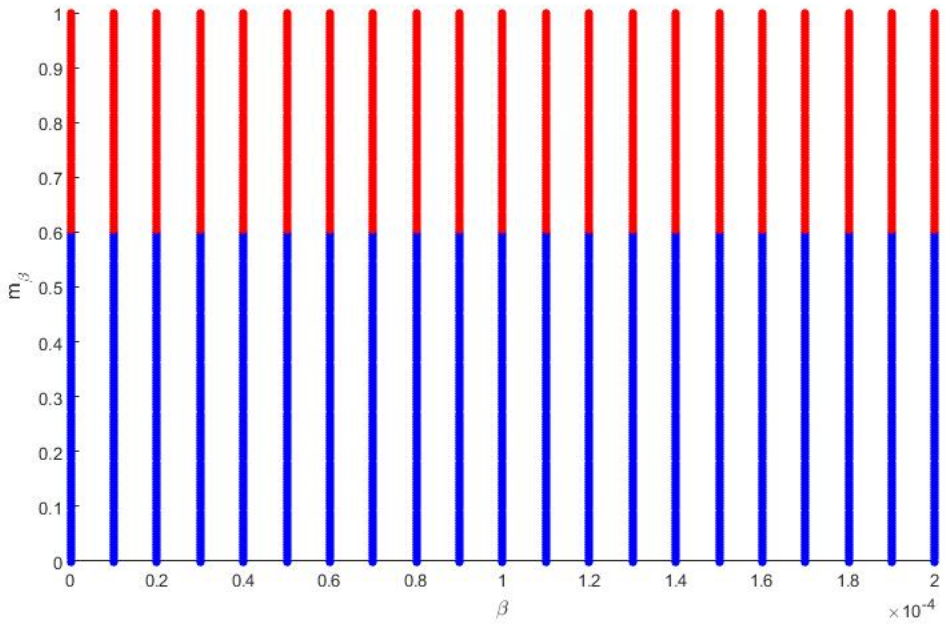

Figure 3.14: m_β vs β in the four-variable system with initial condition of $m_\alpha = 1$ showing manifold.

In the m_α vs α plane, the change to the four-variable system makes SS1 impossible to reach by only changing the initial conditions on m_α and α, as seen in Figures 3.11 and 3.12. Without the boundary between SS1 and SS2, seen in Figure 3.11 but not 3.12, we cannot find initial conditions that lead to SS1 in the four-variable model. In the m_β vs β plane the change to the four-variable system increases the initial amount of m_β needed for the system to converge to SS1, as shown in Figures 3.13 and 3.14. However, the overall form of the manifold in either plane does not change from the seven- to the four-variable system, which is notably gene state independent.

We then examined the effects of different initial conditions on the seven-variable system. To do this we examined the projected manifolds in the m_β vs m_α plane and identified the manifolds by plotting the boundaries between the basins of attraction in Figure 3.15.

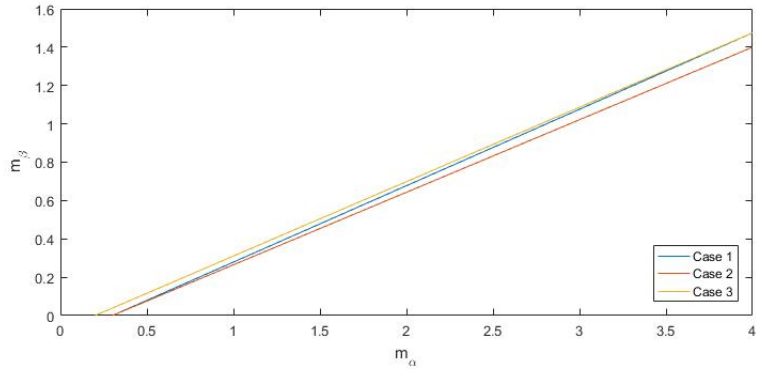

Figure 3.15: Projected manifolds in the m_β vs m_α plane in the seven-variable system with Case 1: all initial conditions at 0, Case 2: initial conditions $A = B = 0$ and α, β, β^R at quasi-steady state values, Case 3: initial conditions $A = B = \beta^R = 0$ and $\alpha = \beta = 1$.

The difference between all three cases is negligible. Whether *apt* and *slbo* genes start as fully inactive or fully active has little effect on the steady state reached from various m_β and m_α initial conditions. Similarly, Case 2 shows that when α, β, and β^R start at quasi-steady state values there is little to no change. Overall, the initial conditions of α, β, and β^R have much less influence on the outcome of the system than the initial conditions of A, B, m_α, or m_β do. This also indicates that α, β, and β^R quickly reach equilibria, reinforcing our decision to make the reduction to a four-variable system.

Next, we tested to see what change in STAT could make the manifolds of the reduced systems match those of the seven-variable system. For the four-variable system, increasing STAT recovered almost the exact same manifold as in the seven-variable system as seen in Figure 3.16.

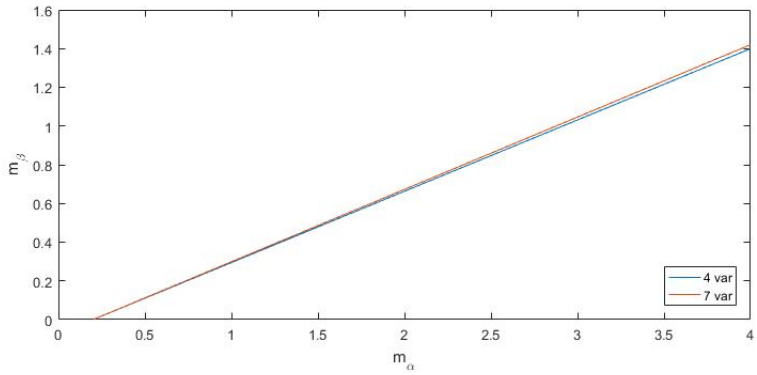

Figure 3.16: Projected manifolds in the m_β vs m_α plane with all initial conditions at 0 in the four-variable system with $S_2^* = 1.3$ and the seven-variable system with $S_2^* = 1$.

In the two-variable systems, changing STAT alone can not recover the exact manifold in the seven-variable system. The dynamic protein model compared to the seven-variable model (see Figure 3.17) is a better fit than the dynamic mRNA model (see Figure 3.18) as expected from the parameter values. $k_{m_\alpha} = 0.54 > 0.298 = k_A$ and $\delta_{m_\alpha} = 0.086 > 0.04 = \delta_A$, and similarly for SLBO. Thus, a quasi-steady state approximation for m_α and m_β is more credible. The manifolds and effects of changing STAT in the two-variable systems indicate that the dynamic protein model is the better approximation.

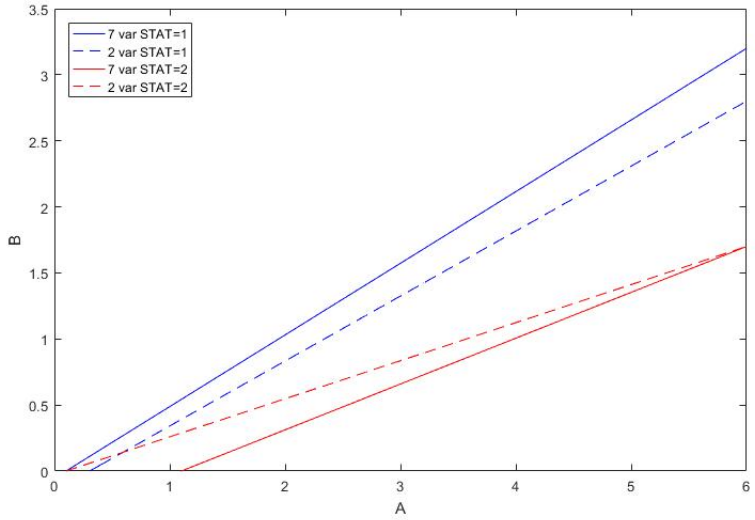

Figure 3.17: B vs A in the dynamic protein and seven-variable system with all initial conditions at 0. The dynamic protein model almost matches the seven-variable model.

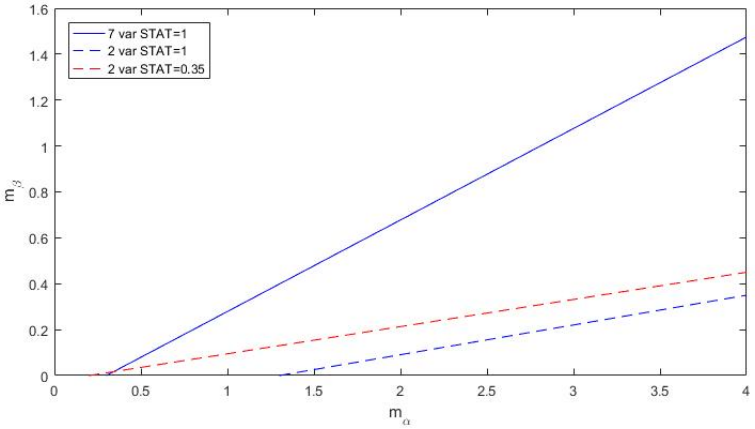

Figure 3.18: m_β vs m_α in the dynamic mRNA and seven-variable system with all initial conditions at 0. The dynamic mRNA model can not match the seven-variable model even with a shift in S_2^*. The boundary between steady states in the seven-variable model for $S_2^* = 0.35$ does not exist for these initial conditions.

4

Dynamic STAT Model

4.1 Developing the Reduced Model

After establishing the cross-repressional system of APT and SLBO we reintroduced STAT dynamics to the model. In order to do this, we reduced the 15-variable system (described in Appendix A.1) to a four-variable system in A, B, S, and S_2^*. We already reduced the seven-variable APT and SLBO system to a two-variable system. Now we reduce the eight-variable STAT activation system through a number of assumptions.

First, we ignored the theoretical APT-STAT complex (c_2) as its effects of APT sequestering STAT are not essential to bifurcation. Then we used the Michaelis-Menten approximation for the activated JAK (J^*) conversion of two STAT molecules to an activated STAT dimer (S_2^*). This eliminates the JAK-STAT complex (c_1) and condenses the conversion. We assumed conservation of JAK to eliminate unactivated JAK (J) by letting $J_T = J + J^*$. We also assumed that UPD (U) activation of JAK is fast relative to STAT activation so activated JAK can be solved for by a quasi-steady state approximation. Lastly, similar to the reduction in the previous chapter, inactive STAT gene (σ) and STAT mRNA (m_σ) were also solved for by quasi-steady state approximations. These assumptions gave us the following additional approximations:

$$\sigma = \frac{1}{\frac{S_2^*}{K_\sigma}+1} \text{ with } K_\sigma = \frac{k_\sigma^b}{k_\sigma^f} \tag{4.1}$$

$$v_{max} = k_{c_1} J^* \tag{4.2}$$

$$k_m = \sqrt{\frac{k_{c_1}^b + k_{c_1}}{k_{c_1}^f}} \tag{4.3}$$

$$J^* = \frac{k_{UJ}^f U J_T}{k_{UJ}^b + k_{UJ}^f U} \tag{4.4}$$

Thus producing a model in A, B, S, and S_2^*:

$$\frac{dA}{dt} = k_A \frac{k_{m_\alpha}(\alpha^*) + m_\alpha^o}{\delta_{m_\alpha} + \delta_{B\alpha} B^2} - \delta_A A \tag{4.5}$$

$$\frac{dB}{dt} = k_B \frac{k_{m_\beta}(\beta^*) + m_\beta^o}{\delta_{m_\beta} + \delta_{A\beta} A} - \delta_B B \tag{4.6}$$

$$\frac{dS}{dt} = -2\frac{v_{max} S^2}{S^2 + k_m^2} + 2k_{S_2^*} S_2^* + k_S \frac{k_{m_\sigma}(1-\sigma) + m_\sigma^o}{\delta_{m_\sigma} + \delta_{A\sigma} A} - \delta_S S \tag{4.7}$$

$$\frac{dS_2^*}{dt} = -k_{S_2^*} S_2^* + \frac{v_{max} S^2}{S^2 + k_m^2} \tag{4.8}$$

4.2 Analysis of Dynamic STAT Model

The seven-, four- and two-variable models with STAT as a parameter have identical bifurcation diagrams, shown in Figure 2.1. The four-variable dynamic STAT model, equations (4.5)-(4.8), has UPD as the bifurcation parameter, but matches the qualitative characteristics of the bifurcations against STAT. The STAT values of the limit points in the dynamic STAT model (0.03618 and 52.84) are very close to the STAT values of the limit points in the other bifurcations (0.0306 and 47.05). Additionally, the S_2^* bifurcation shows that if UPD begins at a high level in

a cell, the cell will remain in the motile state even as UPD decreases to a very low level. Verifying this result experimentally would be a valuable test of the model. Bifurcations of APT and S_2^* against UPD are seen in Figures 4.1 and 4.2.

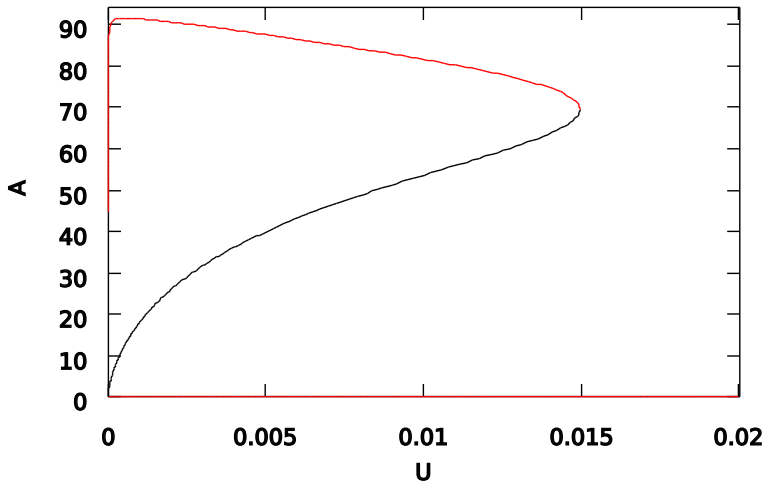

Figure 4.1: Bifurcation of APT against UPD in the dynamic STAT model. Qualitatively similar to APT bifurcation against S_2^*.

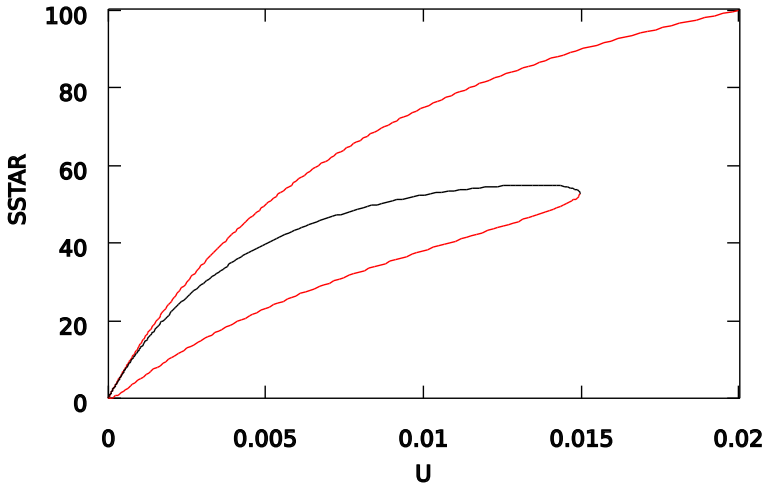

Figure 4.2: Bifurcation of S_2^* against UPD in the dynamic STAT model. S_2^* values at limit points are close to values in APT bifurcation against S_2^*.

We then tested this model to identify what effect a slow increase of STAT has on the cross-repression system of APT and SLBO. We also examined the decoupled AB and SS_2^* subsystems to understand the full system. To decouple the SS_2^* subsystem, we set the level of APT as a parameter that varied from 0 to 100, based on the values APT reaches in the full model. APT as a parameter represents the initial amount of APT present in a cell. We also made UPD dynamic, setting $\frac{dU}{dt} = 0.0001varU$. This allows UPD to increase slowly and then be fixed at a value (by setting $varU = 0$). This lets us examine the behavior of STAT as UPD increases.

The decoupled AB subsystem is the dynamic protein model ((3.11)-(3.12)). The equilibria of the dynamic protein model (A=0.0061, B=51.0178) and (A=91.0617, B=0.0294) are close to those in the seven-variable model (see Table 3.1). The nullclines, stable manifold, and some trajectories of the dynamic protein model are plotted in Figure 4.3.

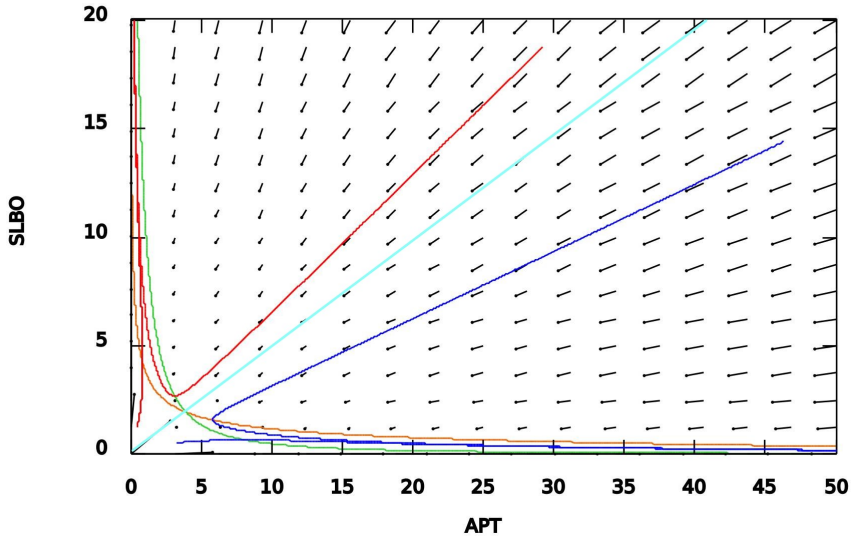

Figure 4.3: AB phase plane, stable manifold, and trajectories in fixed STAT system with $S_2^* = 1$.

The SS_2^* phase plane has just one steady state. This is proven by solving for the S and S_2^* steady states and finding that the discriminant of S is negative for the parameters used (see Appendix A.2 for details). When APT is treated as a parameter, S_2^* loses bistability against UPD as seen in Figure 4.4. Instead, the initial level of APT determines the cell fate.

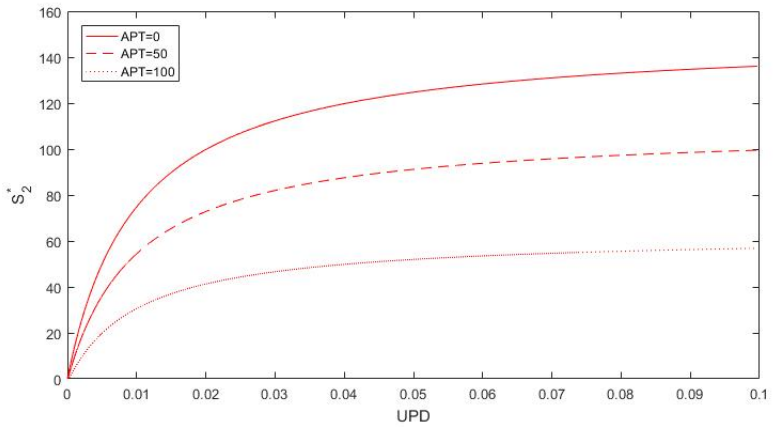

Figure 4.4: Bifurcation of S_2^* against UPD for various levels of APT. There is no longer bistability in S_2^*. As APT increases the S_2^* level decreases.

Figures 4.5 and 4.6 show that when UPD is made dynamic, trajectories in the SS_2^* plane track to the steady state indicated by the intersection of the nullclines. For a given level of UPD, as the value of APT decreases the steady state values of S and S_2^* increase. This moves the system from the stationary (APT dominating) to the motile (SLBO dominating) state. As UPD decreases, S_2^* decreases as well.

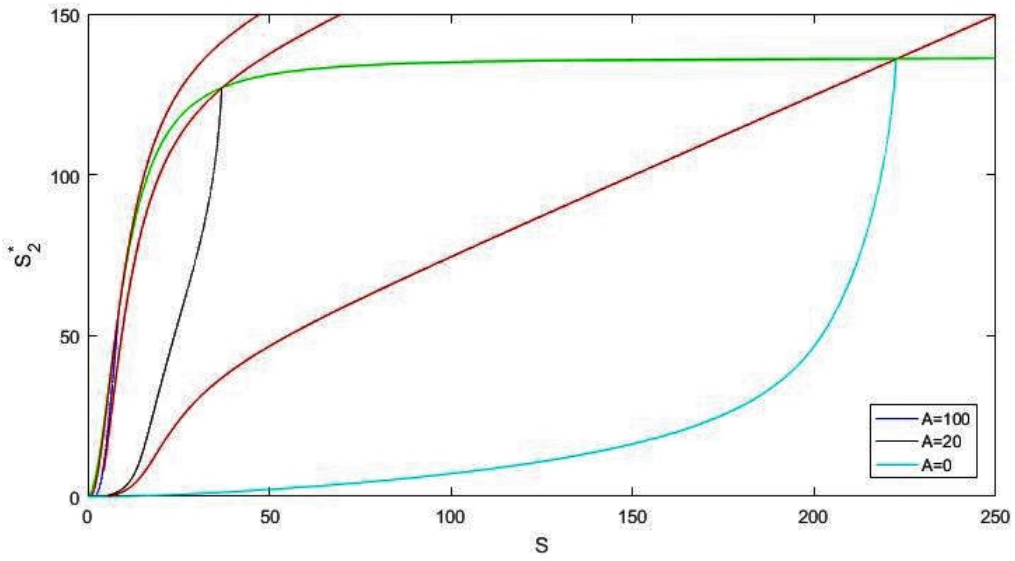

Figure 4.5: Trajectories and nullclines in SS_2^* phase plane with UPD=0.1. Green curve is the S_2^* nullcline, red curves are the S nullclines for APT values corresponding with the intersecting trajectory. Trajectories track to increasing steady states as APT decreases.

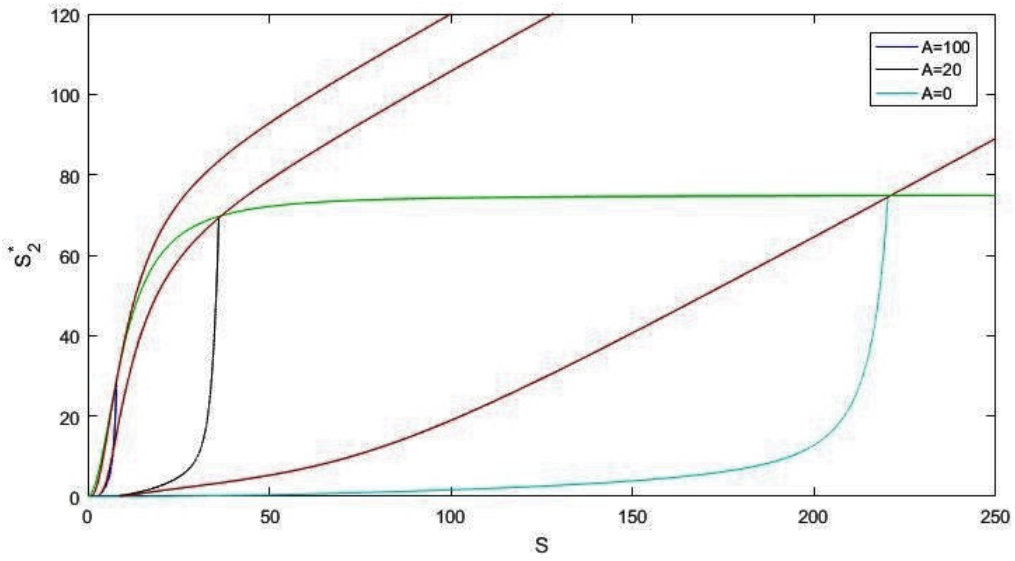

Figure 4.6: Trajectories and nullclines in SS_2^* phase plane with UPD=0.005. Curves as in Figure 4.5. As UPD decreases, S_2^* steady state values decrease while S steady state values remain the same.

Looking at trajectories when UPD is dynamic allows us to better understand the bifurcation diagrams of A and S_2^* against UPD. When UPD is low, the steady state of S_2^* is low and APT dominates. As UPD increases, the steady state of S_2^* passes the threshold needed for SLBO to dominate. Together the AB and SS_2^* subsystems fully explain the bistability in the JAK/STAT pathway.

4.3 Delay from miRNA

APT induced miRNA degradation of STAT is controlled in the model by the parameter $\delta_{A\sigma}$. Figure 4.7 shows time courses of S_2^* for different values of $\delta_{A\sigma}$. In establishing the model we set $\delta_{A\sigma} = 0.05$, which allows S_2^* to equilibrate around

136. This level is well above the threshold needed for the cell to become motile. An increase to $\delta_{A\sigma} = 0.078$ delays STAT activation by a significant amount of time, about 800 min. If we increase $\delta_{A\sigma}$ to just 0.08, S_2^* only reaches a level of around 43 within 1000 minutes. This is below the threshold and thus the cell is stationary. Figure 4.7 shows these three time courses. Each represents a different outcome of the JAK/STAT pathway: GO, where SLBO dominates ($\delta_{A\sigma} = 0.05$); STOP, where APT dominates ($\delta_{A\sigma} = 0.08$); and SLOW, where the transition to motility is delayed ($\delta_{A\sigma} = 0.078$). Since the mechanisms of how APT-activated miRNAs affect STAT are still being analyzed [16] this range in the rate of degradation would be interesting to test experimentally. Delays in STAT activation and failure of activation are possible within a realistic time frame.

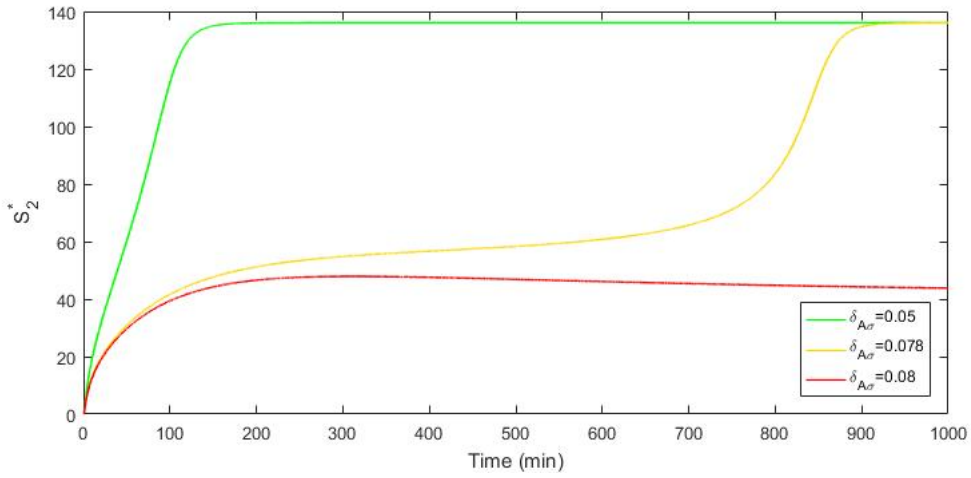

Figure 4.7: Time courses of S_2^* for three levels of miRNA control by $\delta_{A\sigma}$: GO $\delta_{A\sigma} = 0.05$, STOP $\delta_{A\sigma} = 0.08$, SLOW $\delta_{A\sigma} = 0.078$. An increase in $\delta_{A\sigma}$ dramatically delays the level of S_2^* or even stops the transition to motility.

In Figures 4.8-4.10 we get a better picture of the model's behavior for each of the three cell fates. Figure 4.8 shows a 3D plot of S_2^*, APT, and SLBO. Here we can see that in the SLOW cell fate APT increases significantly before dropping off. This is further explored in Figures 4.9 and 4.10. In the SLOW cell fate the level of APT in the cell rises to a fairly high level for a significantly long amount of time. It is only after the level of APT decreases that the level of SLBO begins to converge to its steady state value.

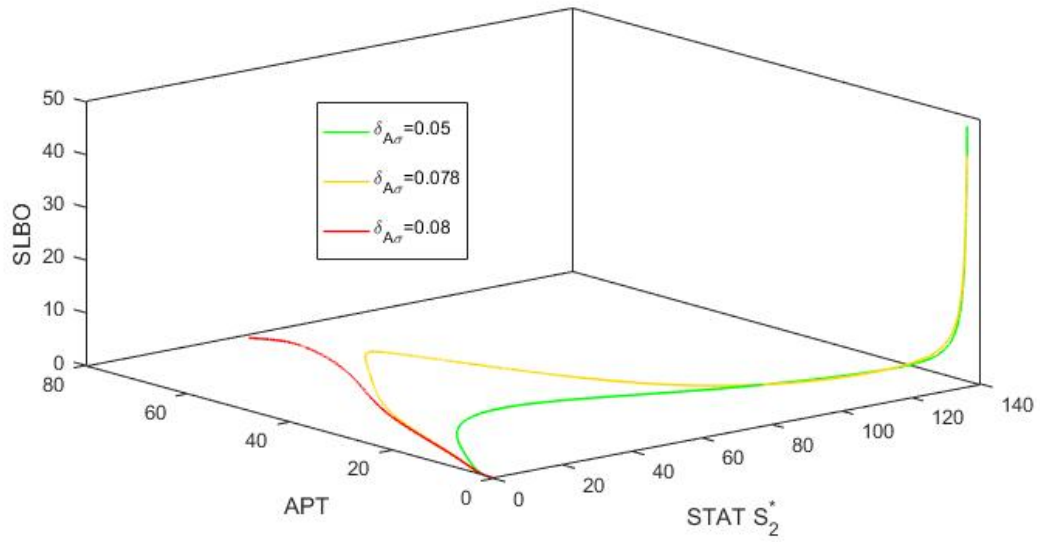

Figure 4.8: 3D plot of S_2^*, APT, and SLBO for the three cell fates described in Figure 4.7. In the SLOW cell fate APT increases significantly before dropping off.

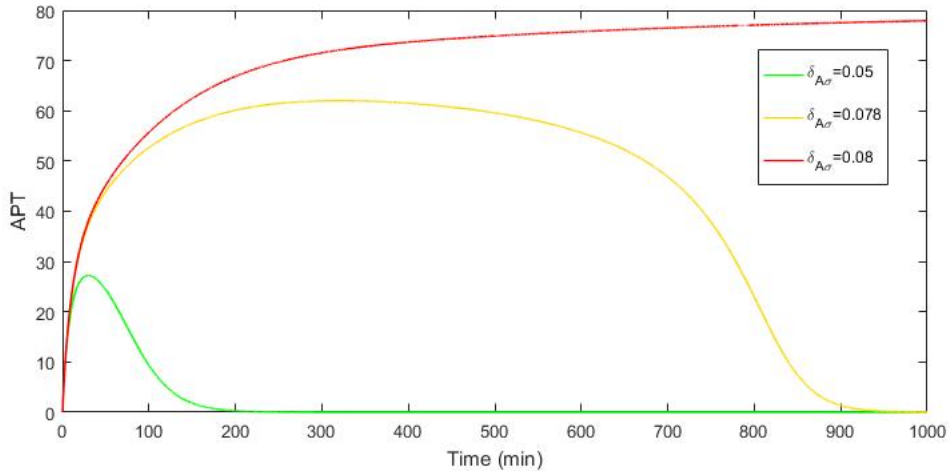

Figure 4.9: Time courses of APT for the three cell fates described in Figure 4.7.

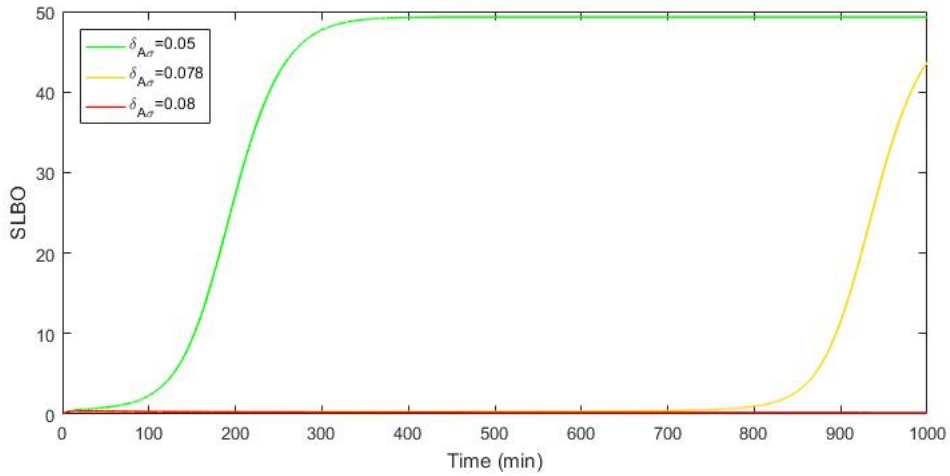

Figure 4.10: Time courses of SLBO for the three cell fates described in Figure 4.7.

5

Experimental Tests

Lastly, we tested our models to see if they reproduced certain behaviors identified in various experiments. It has been shown that if STAT is blocked by stage 9 of cell migration, the level of APT protein drops by about half [12]. It is also known that the activation of STAT by JAK occurs much faster than the action of STAT on APT or SLBO [13]. Additionally, increasing the initial condition of APT should decrease the level of STAT [12]. These behaviors should be achievable by our models.

Both the dynamic protein model and the four-variable dynamic STAT model reproduce the experimental behavior of APT when $S_2^* = 0$, as shown in Figures 5.1 and 5.2. In the dynamic protein model, setting $S_2^* = 0$ causes APT to converge to an equilibrium roughly half that of the stationary steady state. In the four-variable dynamic STAT model, setting $U = 0$ causes STAT to be constantly zero. This again causes APT to converge to an equilibrium roughly half that of the stationary steady state.

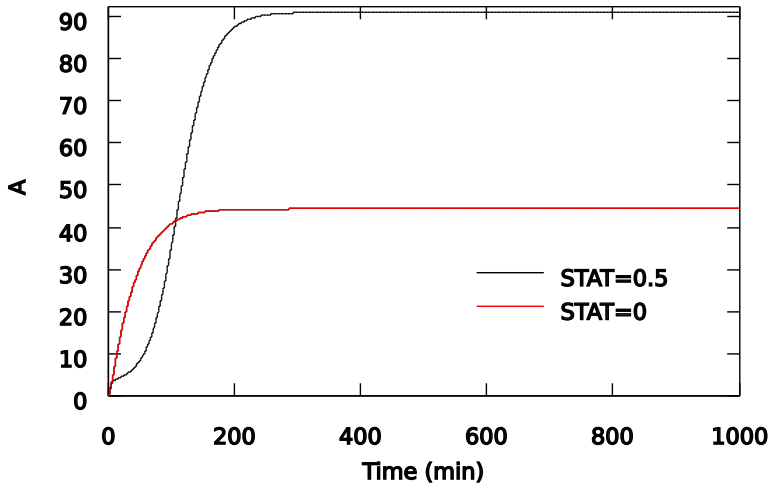

Figure 5.1: Time courses of APT in dynamic protein model. When S_2^*=0 APT decreases by half.

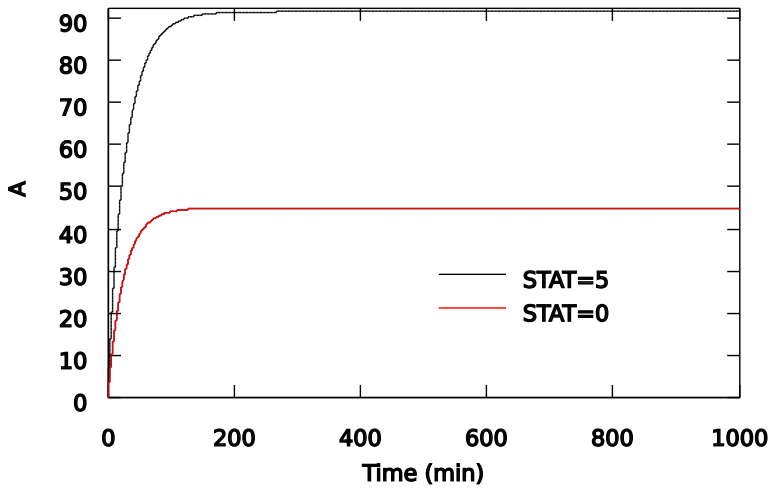

Figure 5.2: Time courses of APT in four-variable dynamic STAT system. When S_2^*=0 APT decreases by half.

As stated previously, the dynamics of STAT production are known to occur much faster than the dynamics of STAT activating APT and SLBO. This supports the cross-repressional models' treatment of STAT as a parameter. This behavior is

seen as well in the dynamic STAT model in Figures 5.3 and 5.4. APT and SLBO begin to converge faster after STAT reaches equilibrium. This is more apparent for SLBO which is consistent with the fact that APT can also be activated by EYA.

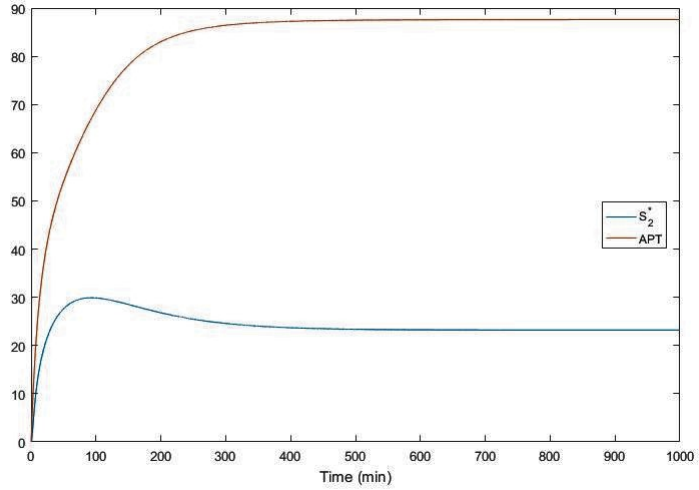

Figure 5.3: Time courses of S_2^* and APT. APT converges faster after S_2^* reaches equilibrium.

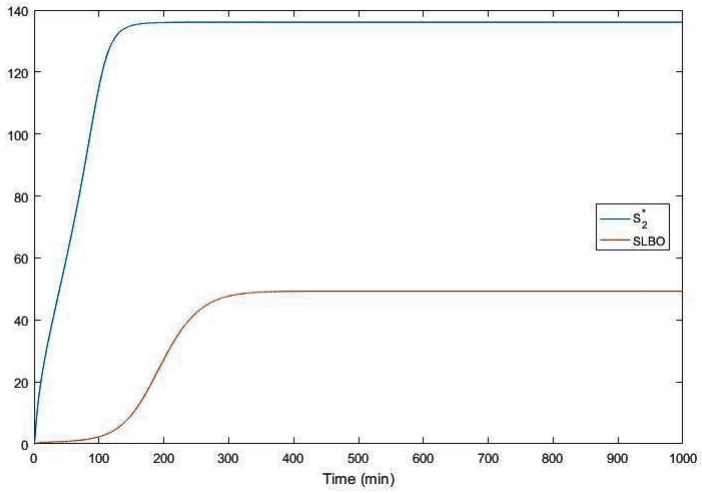

Figure 5.4: Time courses of S_2^* and SLBO. SLBO begins to converge after S_2^* reaches equilibrium.

APT acts as an inhibitor to STAT activity, so for higher APT initial conditions we should see lower levels of STAT. This occurs in the 15-variable model (Figure 5.5) but not in the reduced dynamic STAT model (Figure 5.6). If we lower the value of UPD in the dynamic STAT model, we do see a decrease in the level of S_2^* (Figure 5.7). However, this decrease is only observed for certain values of UPD and does not fully match the behavior of the 15-variable model. This indicates that the feedback inhibition of STAT by APT is not being fully represented in the four-variable dynamic STAT model.

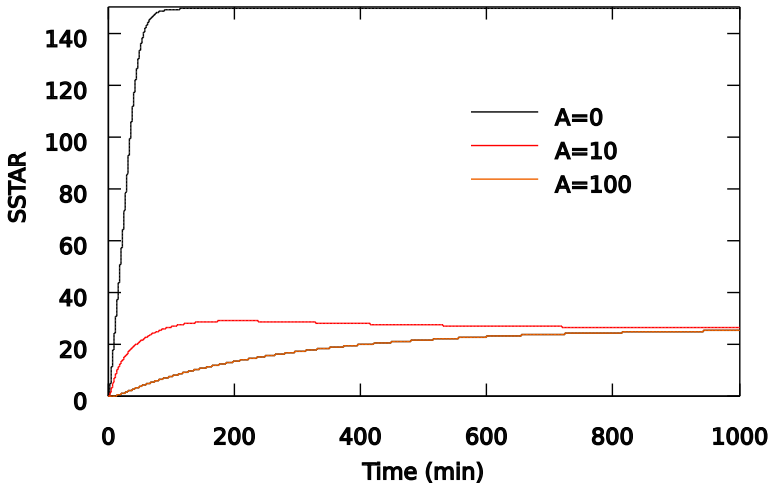

Figure 5.5: Time courses of S_2^* with UPD=0.1 for initial conditions of APT in 15-variable system with all other initial conditions at 0. As APT increases STAT decreases, as seen in experiments.

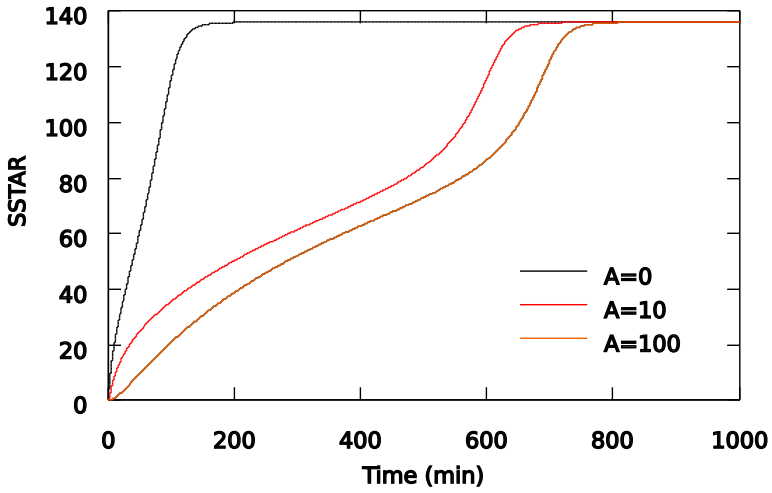

Figure 5.6: Time courses of S_2^* with UPD=0.1 for initial conditions of APT in dynamic STAT system. As APT increases, STAT remains the same.

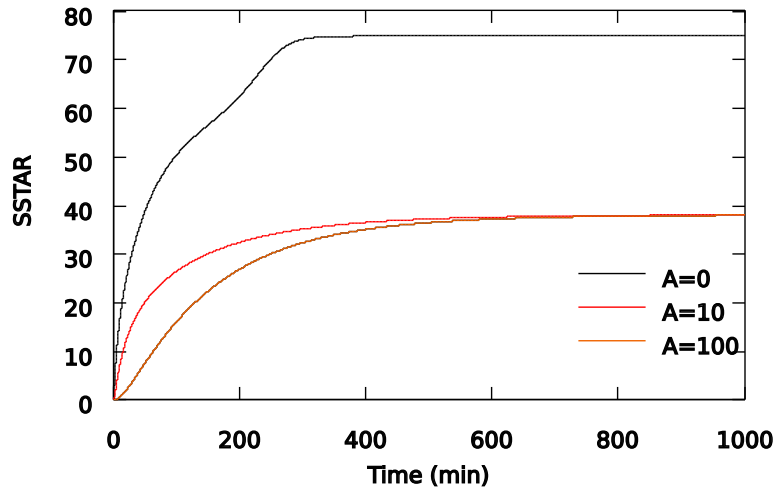

Figure 5.7: Time courses of S_2^* with UPD=0.01 for initial conditions of APT in dynamic STAT system. As APT increases, STAT decreases but does not completely match the behavior of the 15-variable system.

By returning to the 15-variable model and testing each of the reductions made to develop the four-variable dynamic STAT model, we identified the quasi-steady state assumption made for the variables β and β^R as creating this discrepancy

between the 15- and four-variable dynamic STAT models. It is interesting to note that the discrepancy comes from a reduction in the SLBO dynamics and not a reduction in the STAT dynamics.

6

Discussion

From the mechanistic Ge and Stonko model, we first reduced the cross-repression system of APT and SLBO to a two-variable model with only APT and SLBO as dynamic. We then reduced the system of STAT activation to a two-variable model with only STAT and activated STAT as dynamic. We combined the two models into a four-variable model. This allowed us to fully understand bistability in the JAK/STAT pathway. Critically, both the models with dynamic and fixed STAT display the bistability of the stationary and motile cell states expected from experimental data for medium saturation of STAT.

We established parameters that proved bistability was obtainable under realistic conditions. Every parameter in the seven-variable model was found to have a wide range of values that guaranteed bistability. The robustness of the parameters also suggests the biophysical utility of the model. Cell migration is an essential biological process, and as such is likely to be robust as indicated by the model. It makes sense that the JAK/STAT pathway would be able to operate successfully under a range of parameter values.

Ge and Stonko concluded that the key aspect necessary for bistability in APT and SLBO is cooperativity in SLBO repressing APT mRNA. In our dynamic STAT model, we found that the feedback inhibition of APT on STAT is necessary for

bistability in STAT coming from the bistability between APT and SLBO. We also found that the initial amount of APT present in a cell is a major factor in whether or not the cell will become motile through affecting the level of STAT activity. Both the fixed and dynamic STAT models also reproduce behavior seen in experiments. However, it seems as thought the quasi-steady state reduction in the variables β and β^R causes a discrepancy in the behavior of the 15- and four-variable dynamic STAT models. We would like to further explore why this reduction affects the dynamics of STAT when the initial conditions of APT are increased.

We also showed that delays in STAT activation and failure of activation are possible within a realistic time frame. By controlling the degree of feedback inhibition of APT on STAT we can induce a delay in the transition to cell motility or cause the cell to remain stationary. This result is due to the proximity of the critical UPD level to a limit point bifurcation.

The limitations of this model are mainly due to the assumptions made in the development. The dynamic protein model was reduced from the seven-variable model under certain time scale assumptions, some of which have more data supporting them than others. The STAT dynamics were also reduced under a number of assumptions. One assumption was the decision to ignore the c_2 equation, which allows APT to act as a buffer on STAT. Since the action of APT on STAT is known to function by preventing activation through miRNAs [16] as well as limiting protein production [12], this assumption might oversimplify the larger system.

As manifolds in higher dimensions are difficult to find algebraically, we chose to visually identify two-dimensional projections of the full manifolds. In the dynamic STAT model, it would be useful in future work to reduce the system to two or three variables so the manifold could be found. One possible way of achieving this would be to assume conservation of STAT so that $S_T = S + 2S_2^*$. We would then be able to solve algebraically for the manifold between the stationary and motile steady states and better understand how aspects of the system affect the manifold.

Future work should use experimental data to test the assumptions and conclusions made for this model. Further study into the various methods by which APT inhibits STAT would enable us to improve how the model captures this interaction. We would also like to expand on how APT and SLBO interact through miRNAs. Both of these interactions directly affect bistability in the model, so should be explored further. Experiments with controlling the level of UPD secreted could identify how quickly the signal enters border cells and the exact levels of UPD which correspond with the activated STAT threshold to induce motility. It would also be valuable to know the level of APT present in border cells through activation by EYA.

The JAK/STAT signalling pathway is known to be well conserved. Specifically, it seems to be comparable in *Drosophila* and in humans. Thus as the model we have developed helps to explain cell motility in *Drosophila*, it should also add to our understanding of the process in humans.

A.1 15 Variable Model

Ge and Stonko created a 15 variable model to capture the mechanisms of the JAK/STAT signalling pathway. The variables not present in the seven-variable model are defined in Table 1.

Variable	Description
J^*	Activated JAK
J	JAK
S	STAT monomer
c_1	J^* and S complex
c_2	S_2^* and A complex
S_2^*	Activated STAT dimer
m_σ	STAT mRNA
σ	STAT DNA

Table 1: 15-variable system variables

The system of differential equations:

$$\frac{dJ^*}{dt} = k^f_{UJ}UJ - k^b_{UJ}J^* - k^f_{c_1}J^*S + k^b_{c_1}c_1 + k_{c_1}c_1 \quad (1)$$

$$\frac{dJ}{dt} = -k^f_{UJ}UJ + k^b_{UJ}J^* \quad (2)$$

$$\frac{dS}{dt} = -2k^f_{c_1}J^*S + 2k^b_{c_1}c_1 + 2k_{S_2^*}s_2^* + k_s m_\sigma - \delta_S S \quad (3)$$

$$\frac{dc_1}{dt} = k^f_{c_1}J^*S^2 - k^b_{c_1}c_1 - k_{c_1}c_1 \quad (4)$$

$$\frac{dc_2}{dt} = k^f_{S_2^*A}S_2^*A - k^b_{S_2^*A}c_2 \quad (5)$$

$$\frac{dS_2^*}{dt} = k_{c_1}c_1 - k_{S_2^*}S_2^* - k^f_{S_2^*A}S_2^*A + k^b_{S_2^*A}c_2 \quad (6)$$

$$\frac{dA}{dt} = k_A m_\alpha - \delta_A A - k^f_{S_2^*A}S_2^*A + k^b_{S_2^*A}c_2 \quad (7)$$

$$\frac{dB}{dt} = k_B m_\beta - \delta_B B \tag{8}$$

$$\frac{dm_\alpha}{dt} = k_{m_\alpha}(1-\alpha) - \delta_{m_\alpha} m_\alpha + m_\alpha^o - \delta_{B\alpha} B^2 m_\alpha \tag{9}$$

$$\frac{dm_\beta}{dt} = k_{m_\beta}(1-\beta-\beta^R) - \delta_{m_\beta} m_\beta + m_\beta^o - \delta_{A\beta} A m_\beta \tag{10}$$

$$\frac{dm_\sigma}{dt} = k_{m_\sigma}(1-\sigma) - \delta_{m_\sigma} m_\sigma + m_\sigma^o - \delta_{A\sigma} A m_\sigma \tag{11}$$

$$\frac{d\alpha}{dt} = -k_\alpha^f S_2^* \alpha + k_\alpha^b (1-\alpha) \tag{12}$$

$$\frac{d\beta}{dt} = -k_\beta^f S_2^* \beta + k_\beta^b (1-\beta-\beta^R) \tag{13}$$

$$\frac{d\beta^R}{dt} = k_{\beta^R}^f A\beta - k_{\beta^R}^b \beta^R \tag{14}$$

$$\frac{d\sigma}{dt} = -k_\sigma^f S_2^* \sigma + k_\sigma^b (1-\sigma) \tag{15}$$

$$\tag{16}$$

The parameters values used in the dynamic STAT system are listed in Table 2.

Parameter	Value	Units
k_{UJ}^{f}	10	min^{-1}
k_{UJ}^{b}	0.1	nM*min^{-1}
$k_{c_1}^{f}$	1	min^{-1}
$k_{c_1}^{b}$	0.1	nM*min^{-1}
k_{c_1}	100	nM*min^{-1}
$k_{S_2^*}$	0.1	nM^{-1}*min^{-1}
k_S	3	min^{-1}
δ_S	0.1	min^{-1}
k_{m_σ}	1	min^{-1}
δ_{m_σ}	0.2	min^{-1}
m_σ^o	0.5	nM*min^{-1}
$\delta_{A\sigma}$	0.05	nM^{-1}*min^{-1}
k_σ^f	1	min^{-1}
k_σ^b	2	nM*min^{-1}
J_T	0.15	nM

Table 2: Dynamic STAT system parameters

A.2 Finding the discriminant of S

The four variable dynamic STAT model:

$$\frac{dA}{dt} = k_A \frac{k_{m\alpha}(1-\alpha) + m_\alpha^o}{\delta_{m\alpha} + \delta_{B\alpha}B^2} - \delta_A A \tag{17}$$

$$\frac{dB}{dt} = k_B \frac{k_{m\alpha}(\beta^*) + m_\beta^o}{\delta_{m\beta} + \delta_{A\beta}A} - \delta_B B \tag{18}$$

$$\frac{dS}{dt} = -2\frac{v_{max}S^2}{S^2 + k_m^2} + 2k_{S_2^*}S_2^* + k_S \frac{m_\sigma^o + k_{m\sigma}(1-\sigma)}{\delta_{m\sigma} + \delta_{A\sigma}A} - \delta_S S \tag{19}$$

$$\frac{dS_2^*}{dt} = \frac{v_{max}S^2}{S^2 + k_m^2} - k_{S_2^*}S_2^* \tag{20}$$

We isolate the SS_2^* system and set it to steady state. For equation (20) we get

$$S_2^* = \frac{v_{max}}{k_{S_2^*}} \frac{S^2}{S^2 + k_m^2}.$$

This leaves us with

$$0 = k_S \frac{m_\sigma^o + k_{m\sigma}(1-\sigma)}{\delta_{m\sigma} + \delta_{A\sigma} A} - \delta_S S \tag{21}$$

after plugging the expression for S_2^* into (19).

We use the expression for σ in terms of S_2^* to get the active *stat* gene level

$$(1-\sigma) = \frac{S_2^*}{S_2^* + k_\sigma} = \frac{\frac{v_{max}}{k_{S_2^*}} \frac{S^2}{S^2+k_m^2}}{\frac{v_{max}}{k_{S_2^*}} \frac{S^2}{S^2+k_m^2} + k_\sigma} = \rho \frac{S^2}{S^2 + \kappa}$$

where $\rho = \frac{r}{r+1}$ and $\kappa = \frac{k_m^2}{r+1}$ with $r = \frac{v_{max}}{k_\sigma k_{S_2^*}}$.

Plugging this into 21 we get

$$0 = m_\sigma^o + k_{m\sigma} \rho \frac{S^2}{S^2 + \kappa} - \frac{\delta_S}{f} S \tag{22}$$

where $f = \frac{k_S}{\delta_{m\sigma} + \delta_{A\sigma} A}$. Simplifying yields

$$aS^3 + bS^2 + cS + d = 0 \tag{23}$$

where $a = -\frac{\delta_S}{f}, b = m_\sigma^o + k_{m\sigma}\rho, c = -\frac{\delta_S}{f}\kappa$, and $d = m_\sigma^o \kappa$.

Now the discriminant, $\Delta = b^2c^2 - 4ac^3 - 4b^3d - 27a^2d^2 + 18abcd$, tells us the number of real steady states (3 if $\Delta > 0$, 1 if $\Delta < 0$).

$$\Delta = 20 m_\sigma^o k_{m_\sigma} \rho \left(\kappa \frac{\delta_S}{f}\right)^2 + \left(k_{m_\sigma} \rho \kappa \frac{\delta_S}{f}\right)^2 \tag{24}$$

$$-4\left[m_\sigma^{o\,4}\kappa + 3 m_\sigma^{o\,3} k_{m_\sigma}\rho\kappa + 2\left(m_\sigma^o \kappa \frac{\delta_S}{f}\right)^2 + 3\kappa\left(m_\sigma^o k_{m_\sigma}\rho\right)^2 + m_\sigma^o \kappa \left(k_{m_\sigma}\rho\right)^3 + \kappa^2 \left(\frac{\delta_S}{f}\right)^4\right] \tag{25}$$

Since the parameters are all positive, the discriminant is always negative.

Bibliography

[1] G.-H. Baeg. "Genome-wide RNAi analysis of JAK/STAT signaling components in Drosophila". In: *Genes & Development* 19.16 (2005), pp. 1861–1870.

[2] Xuan Ge and David Stonko. "Modelling a Cellular Response to a Gradient". In: *UMBC Review* 13 (2012), pp. 92–113.

[3] Nicholas J. Guido et al. "A bottom-up approach to gene regulation". In: *Nature* 439.7078 (2006), pp. 856–860.

[4] Stephen E. Halford and John F. Marko. "How do site-specific DNA-binding proteins find their targets?" In: *Nucleic Acids Research* 32.10 (2004), pp. 3040–3052.

[5] J. L. Hargrove, M. G. Hulsey, and E. G. Beale. "The kinetics of mammalian gene expression". In: *BioEssays: News and Reviews in Molecular, Cellular and Developmental Biology* 13.12 (Dec. 1991), pp. 667–674.

[6] Robin E. Harris et al. "Brat Promotes Stem Cell Differentiation via Control of a Bistable Switch that Restricts BMP Signaling". In: *Developmental Cell* 20.1 (2011), pp. 72–83.

[7] Benjamin Lewin. *Genes VIII*. Pearson Prentice Hall, 2004.

[8] Lathiena A. Manning et al. "Tissue landscape alters adjacent cell fates during Drosophila egg development." In: *NATURE COMMUNICATIONS* 6 (2015), p. 7356.

[9] Amanda J. Monahan and Michelle Starz-Gaiano. "Socs36E limits STAT signaling via Cullin2 and a SOCS-box independent mechanism in the Drosophila egg chamber." In: *Mechanisms of Development* 138.Part 3 (2015), pp. 313–327. ISSN: 0925-4773.

[10] Denise J. Montell, Pernille Rorth, and Allan C. Spradling. "Slow border cells, a locus required for a developmentally regulated cell migration during oogenesis, encodes Drosophila C/EBP". In: *Cell* 71.1 (1992), pp. 51–62.

[11] Azita Parsaeian, Monica Olvera de la Cruz, and John F. Marko. "Binding-rebinding dynamics of proteins interacting non-specifically with a long DNA molecule". In: *Physical review. E, Statistical, nonlinear, and soft matter physics* 4 (2013), p. 040703.

[12] Michelle Starz-Gaiano et al. "Feedback Inhibition of JAK/STAT Signaling by Apontic Is Required to Limit an Invasive Cell Population". In: *Developmental Cell* 14.5 (2008), pp. 726–738.

[13] Michelle Starz-Gaiano et al. "Interpretation of the UPD/JAK/STAT morphogen gradient in Drosophila follicle cells". In: *Cell cycle (Georgetown, Tex.)* 8.18 (2009), pp. 2917–2925.

[14] Sunny Trivedi and Michelle Starz-Gaiano. "Drosophila Jak/STAT Signaling: Regulation and Relevance in Human Cancer and Metastasis." In: *INTERNATIONAL JOURNAL OF MOLECULAR SCIENCES* 19.12 (2018).

[15] Edward Yang et al. “Dissociation Time from DNA Determines Transcriptional Function in a STAT1 Linker Mutant”. In: *Journal of Biological Chemistry* 277.16 (2002), pp. 13455–13462.

[16] Wan Hee Yoon, Hans Meinhardt, and Denise J. Montell. “miRNA-mediated feedback inhibition of JAK/STAT morphogen signalling establishes a cell fate threshold”. In: *Nature Cell Biology* 13.9 (2011), pp. 1062–1069.